

# Structure of the Martian Dayside Magnetosphere: Two Types

O. L. Vaisberg<sup>a,\*</sup> and S. D. Shuvalov<sup>a,\*\*</sup>

<sup>a</sup> *Space Research Institute, Russian Academy of Sciences, Moscow, Russia*

\**e-mail: olegv@iki.rssi.ru*

\*\**e-mail: shuvalovsergei@gmail.com*

Received December 28, 2021; revised March 25, 2022; accepted April 13, 2022

**Abstract**—A set of scientific instruments capable of high temporal resolution measurements onboard the Mars Atmosphere and Volatile Evolution (MAVEN) spacecraft made it possible to study the structure and properties of the dayside Martian magnetosphere. The Mars plasma envelope on the dayside of the planet was discovered based on observations on the first orbiters of Mars (Vaisberg et al., 1976; Gringauz et al., 1976). The high temporal and mass resolution of MAVEN instruments made it possible to study the structure and processes in the plasma of the dayside magnetosphere, the plasma layer that exists between the solar wind heated by the shock wave and the ionosphere (Vaisberg et al., 2017). It is shown that, under different external conditions, two different types of plasma layers are formed between the ionosphere and magnetosheath on the dayside of the planet: (1) mixture of heated ionospheric ions and picked-up exospheric ions and (2) a layer of ionospheric ions accelerated by the solar wind motional electric field called “plume” (Dong et al., 2015). The first type of the Martian daytime magnetosphere is formed as a result of the interaction of oxygen exospheric ions captured and accelerated by the solar wind with the upper part of the Martian ionosphere (Vaisberg and Shuvalov, 2021). The second type of the Martian dayside magnetosphere is formed by the acceleration of an ion beam from the outer ionosphere, which then passes into a more energetic plume beam in the magnetosheath. This article discusses typical plasma populations, their properties and conditions that lead to the formation of the daytime magnetosphere from the material of the upper ionosphere.

**Keywords:** Mars, magnetosphere, solar wind, plume, pickup, MAVEN

**DOI:** 10.1134/S0038094622050069

The first close flyby of Mariner-4 near Mars on July 14–15, 1964 at a minimum distance of 13300 km showed that Mars does not have a strong magnetic field, and the solar wind can directly interact with its atmosphere (Dryer and Heckman, 1967).

The first crossings of the Martian magnetosphere were carried out by the *Mars-2*, *Mars-3* and *Mars-5* spacecraft in the 1970s and found an increase in the magnetic field up to ~30 nT (Dolginov et al., 1976) and the presence of ions with a lower energy than in the magnetosphere, both on the dayside and well downstream (Bogdanov and Vaisberg, 1975). Unlike Earth, Mars lacks its own global magnetic field, making the Martian plasma environment much smaller. In the early years of space exploration, it was thought that the obstacle to the solar wind was formed by the magnetic field from ionospheric currents induced by the motional electric field of the solar wind. (see e.g., Dessler, 1968).

The term “Martian magnetosphere” was first introduced at the beginning of Mars exploration (Van Allen et al., 1965) and was used to describe the Martian magnetospheric tail, while the dayside magnetosphere remained unexplored for a long time. The region between magnetosheath and ionosphere was

interpreted in terms of existence of a boundary layer on the day side of Mars (Szego et al., 1998). The Mars Express (MEX) spacecraft measured the plasma ion composition in this region (Dubinin et al., 2008a, 2008b). Magnetic pile-up with a discontinuity (called a magnetic compression boundary) was found, although it was absent in some cases. A “boundary” of ionospheric photoelectrons was also observed, often accompanied by a sharp increase (up to  $\sim 10^3 \text{ cm}^{-3}$ ) in the number density of the ionospheric plasma.

Only in September 2014, the Mars Atmosphere and Volatile Evolution (MAVEN) spacecraft, carrying a comprehensive complex of plasma instruments, arrived in Martian orbit and provided an opportunity to study the region between the Martian magnetosheath and ionosphere in detail. There are several works that discuss the structure of the boundary and the processes inside it (Holmberg et al., 2019; Espley, 2018; Halekas et al., 2015, 2018). According to Halekas et al., 2017, “the Martian magnetosphere is formed as a result of direct and indirect interaction of the solar wind with the Martian ionosphere through a combination of induction and mass loading processes.” However, knowledge about the magnetoplasma shell of the dayside of Mars was not enough to understand its

structure and the processes of interaction between the shocked solar wind and the ionosphere. There are many designations of boundaries and envelopes in this part of the Martian magnetoplasma environment, not to mention the processes occurring in this part of the Martian magnetosphere.

In this paper, we consider two different types of the magnetosphere structure between the shocked solar wind and the ionosphere. The first is characterized by the presence of plasma, which is a mixture of picked-up exospheric ions and heated and accelerated ionospheric ions (Vaisberg and Shuvalov, 2021). The second type is characterized by the presence of a layer with low-temperature ionospheric ions accelerated by the electric field of the solar wind and called the “ion plume” (Kallio and Koskinen, 1999; Kallio et al., 2006, 2008, Boesswetter et al., 2007; Dubinin et al., 2006, 2011; Liemohn et al., 2014; Dong et al., 2015). The low-energy part of the plume is located below the boundary of the Martian magnetosphere. In this paper we analyze and compare the structure of both types of magnetosphere structure.

## INSTRUMENTATION

The MAVEN spacecraft arrived at Mars in September 2014 to study processes in the upper atmosphere and ionosphere and their interaction with the solar wind, and for atmospheric losses estimation (Jakosky et al., 2015). MAVEN was set into an elliptical orbit with a periaapsis of approximately 150 km, an apoapsis of 6200 km, and a period of  $\sim 4.5$  h.

The MAVEN instruments measurements data are publically available. Project specialists are happy to answer questions. In this paper we discuss observations primarily made with the Supra-Thermal and Thermal Ion Composition (STATIC) instrument from July to October 2019, during solar minimum. The STATIC instrument, mounted on an Actuated Payload Platform (APP) driven payload platform, is used to study the characteristics of various ions populations as the solar wind interacts with Mars.

The instrument consists of a toroidal electrostatic analyzer with an electrostatic deflector at the entrance, providing a field of view of  $360^\circ \times 90^\circ$ , in combination with a time-of-flight analyzer that separates the main types of ion species ( $H^+$ ,  $He^{++}$ ,  $He^+$ ,  $O^+$ ,  $O_2^+$ ,  $CO_2^+$ ). It measures the energy spectra of ions with different ( $m/q$ ) in the range of 0.1 eV–30 keV with a minimum cadence of 4 s (McFadden et al., 2015). These characteristics allow measuring the particles velocity distribution function and subsequently calculating its moments (number density, bulk velocity and temperature). Data from the STATIC level 2 d1 data product are used to study the distribution function of ions of various masses. This data product contains data on differential energy fluxes for ions in 32 energy steps, 4 polar and 16 azimuth angles for eight different

masses. The cadence of measurements for the time intervals presented in the article is 4 s. At high count rates some proton data can be wrongly registered as ions of bigger masses due to incorrect identification of start/stop signals of the time-of flight scheme. In order to diminish this effect, we applied a special procedure for  $O^+$  and  $O_2^+$  data, in which 8% of protons differential energy flux was subtracted from oxygen ion data for the same energy and angular bins.

Along with STATIC observations we used data obtained by the Solar Wind Ion Analyzer (SWIA, Halekas et al., 2015), a top-hat instrument with  $360^\circ \times 90^\circ$  field of view mounted on the solar array panel, Solar Wind Electron Analyzer (SWEA, Mitchell et al., 2016), and by the measurements of the magnetic field with 32 Hz cadence (MAG, Connerney et al., 2015). For SWIA and SWEA measurements level 2 data products with survey spectra measurements were used, which provide the data with 4 and 2 seconds cadence, respectively.

## OBSERVATIONS

This analysis is based on the observations made on the dayside of the Martian magnetosphere. The used data were selected by the following criteria: (1) during low solar minimum (having more non-disturbed cases for analysis), (2) dayside magnetosphere boundary crossings (3) the regions without crustal magnetic field anomalies (having less additional influences) factors avoiding magnetic disturbances, implying crossings in the northern hemisphere. Altogether 115 crossings of magnetosphere boundary were considered within time interval from July 27, 2019 to October 31, 2019 for solar-zenith angles (SZA) from  $\sim 60^\circ$  to  $\sim 95^\circ$  (Fig. 1). Distribution of SZAs of the observed crossings is given in figure 1. This “landscape” of crossings was classified as: (a) 65 orbits with the ion plume originated within the magnetosphere and extended far to the magnetosheath, and (b) 50 orbits without a plume feature but with the observations of pick-up oxygen ions in the sheath/upper ionosphere and the cold ionospheric component within magnetosphere.

We present a description of two types of formations that separate the magnetosheath flow from the upper ionosphere on the dayside of Mars. As for the two types of layers separating the flow regions of the magnetosheath and the ionosphere on the day side of Mars, their physical causes differ significantly. In this paper, we mainly focus on the dayside magnetosphere of the first type, which relies heavily on the dynamics of ion beams.

## DAYSIDE MAGNETOSPHERE—1ST TYPE

This section considers two samples from 57% of 1st type formations from the total of 115 orbits considered in this paper.

Figure 2 shows the data obtained on July 29, 2019 (03:10:21–03:32:09 UT). MAVEN moved from the magnetosheath to the ionosphere at SZA  $\sim 69.5^\circ$  while crossing the upper boundary of the magnetosphere. We used the following features in identifying the boundary of the magnetosphere:

1a—Reduction of the ion flux of the magnetosheath. Here we have two distinct changes in the proton spectra: at  $\sim 03:17:30$  and at  $\sim 03:20$  UT. The feature observed at  $\sim 03:17:30$  UT is due to the rotation of the platform with the STATIC spectrometer. At  $\sim 03:20$  UT, we observe a splitting of the proton spectra into two components: a low-energy (100–200 eV) component and a high-energy component. Higher energy protons originating from the solar wind and magnetically trapped protons originating from an expanded hydrogen atmosphere can penetrate deeper into the magnetosphere due to their large Larmor radii. The origin of the low-energy component is not so clear. It may consist of shell protons, which gradually lose their momentum, and protons of atmospheric origin, which receive momentum from the solar wind.

1b—The position of the boundary at  $\sim 03:20$  UT is confirmed by measurements with the SWIA instrument, which does not change the viewing direction. The boundary of the induced magnetosphere can be easily determined by a sharp change in the ionic composition, as can be seen in Fig. 1 on the ion spectra, and according to the ratio  $n_p/(n_p + n_h) \approx 0.5$ , where  $n_p$  is the proton concentration, and  $n_h$  is the sum of the number densities of  $O^+$  and  $O_2^+$  ions.

1c—The decrease in the level of magnetic field fluctuations observed at  $\sim 03:20$  UT is consistent with our identification of the boundary.

The third and fourth panels in Fig. 2 show the behavior of oxygen ions. We observe fluxes of  $O^+$  ions with energies of about 100–5000 eV in the magnetosheath. These ions are produced in the oxygen corona and are accelerated by the electric field of the solar wind. They are also visible in the magnetosphere, where some of them have higher energy.  $O^+$  ions with energies below 100 eV and  $O_2^+$  ions with energies of  $\sim 5$ –330 eV are predominantly accelerated at lower altitudes and cannot acquire higher energies.

The two boundaries within the transition from the magnetosheath to the ionosphere can be identified using the plasma and magnetic parameters in Fig. 2. The outer boundary is quite sharp and is determined by a number of physical parameters (going from the magnetosheath to the magnetosphere): a drop in the proton energy flux, a sudden appearance of pick-up ions  $O^+$  and  $O_2^+$  with energies of 3–300 eV, a drop in the electron energy, a sharp drop in the electron temperature, a drop in the ratio  $n_p/(n_p + n_h)$ . The number density of magnetosheath ions drops by an order of magnitude at two boundaries, which determines the

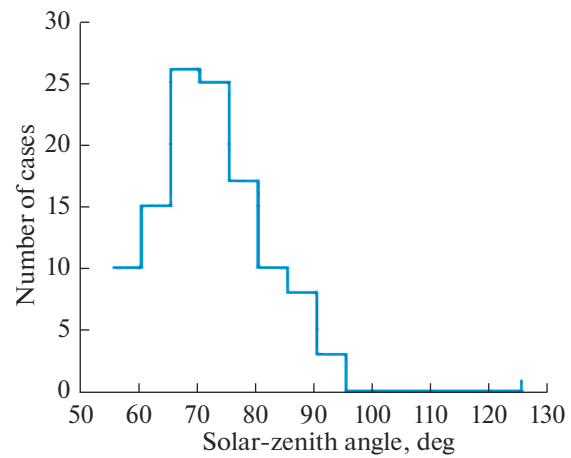
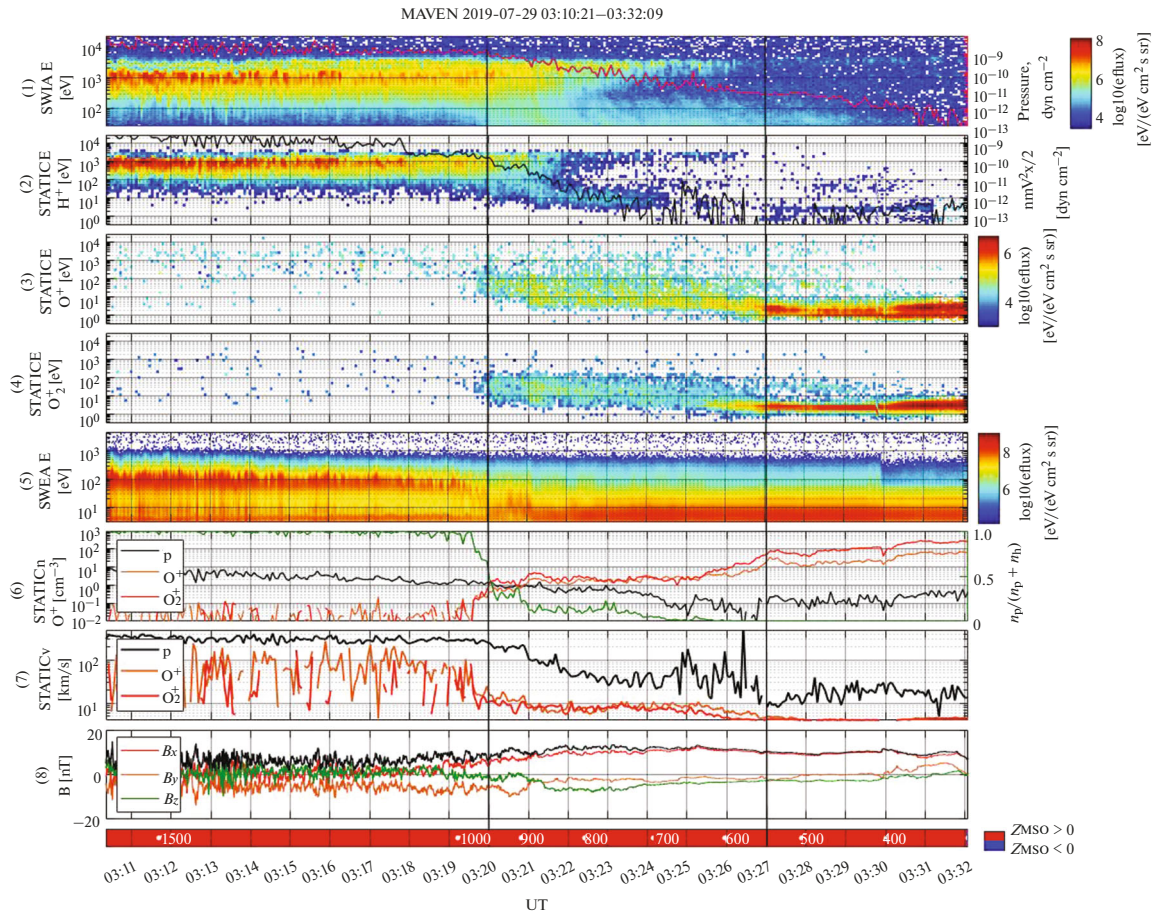


Fig. 1. Distribution of magnetosphere locations by solar-zenith angles for the observed cases. Solar-zenith angle for each crossing was calculated at the time of the magnetopause crossing, defined as  $n_p/(n_p + n_h) \approx 0.5$  based on STATIC measurements.

magnetopause. Some of these boundaries have been discussed by a number of authors. Comparisons of various criteria used to identify the magnetosphere boundary (Holmberg et al., 2019; Espley, 2018; Halekas et al., 2018) show that a sharp drop in solar wind proton pressure by an order of magnitude seems to be the best parameter for identifying the magnetosphere boundary and often coincides with a sharp change in the composition of ions.

The transition from the daytime magnetosphere to the ionosphere occurs quite smoothly and requires additional analysis. For a large concentration range of  $\sim 2$  orders of magnitude, a different role is played, in particular, by the processes of recombination and ionization and a number of other processes, the analysis of which is out of consideration in this work. The following changes in the number density of  $O_2^+$  and  $O^+$  and their ratio are shown in Fig. 2 during the transition from the magnetopause to the ionosphere: (1) the number densities of these ions change from approximately zero to  $\sim 1$ – $2 \text{ cm}^{-3}$  at 03:20:00 and continue until  $\sim 03:25:30$  with minor changes, (2) during the time interval  $\sim 03:25:30$ – $\sim 03:27:20$ , the  $O_2^+$  number densities increase faster than the increase in the  $O^+$  number density and (3) the number densities of the two ions show a small increase with a ratio  $n(O_2^+)/n(O^+) \sim 5$ . The spacecraft entered the ionosphere around  $\sim 03:27:00$  UT, where the cold ion population dominates. The changing ratio  $n(O_2^+)/n(O^+)$  in the magnetosphere will be discussed later as it provides a tool for analyzing the dayside magnetosphere.

Figure 3 shows the angle between the ion bulk velocity and the outer normal to the planet’s surface for  $O^+$  and  $O_2^+$  ions. It can be seen that the ions in the



**Fig. 2.** From top to bottom: (1) time–energy spectrogram integrated over all types of ions; the red line shows ion dynamic pressure  $n^*m^*V^2/2$  assuming that all measured ions are protons, (2–4) energy–time spectrograms for protons,  $O^+$  and  $O_2^+$  ions, (5) electron energy–time spectrogram, (6) number density of protons,  $O^+$ ,  $O_2^+$  and the ratio of proton number density to the sum of number densities of protons and heavy ions  $n_p/(n_p + n_h)$ , (7) bulk velocities of different ion species, (8) three components and magnetic field magnitude in Mars-Sun-Orbit (MSO) coordinate system. Drop in differential energy flux at  $\sim 03:18$  UT in panel 2 is due to the change of STATIC orientation. Absence of ions with energies higher than  $\sim 500$  eV after  $\sim 03:29.30$  UT is associated with a measurement mode change. Data on panels 2, 3, 4, 6, 7 are from STATIC, 1—from SWIA, 5—from SWEA, 8—from MAG. Of the 112 selected magnetospheric boundary crossings in 2019, this type of plasma sheath was observed in about 60% of cases. The two black vertical lines indicate the location of the magnetosphere.

magnetosheath (before  $\sim 03:19:30$  UT) mainly move towards the planet, since the above-mentioned angle is  $>90^\circ$ . This is because the drift velocity of ion particles trapped in the oxygen corona approximately coincides with the velocity of the solar wind. The directions of volumetric velocities of both ion components below the magnetopause remain stable at  $\sim 60^\circ$ – $40^\circ$  relative to the normal to the surface, indicating that they are moving away from the planet. Approximately at 03:27:00 the angle approaches  $80^\circ$ , but the calculation of this angle includes, in addition to the accuracy of the calculated angle, the velocity of the satellite and the inaccuracy of the calculation of the plasma velocity.

Figure 4 shows the selection of two-dimensional velocity distributions of  $O^+$  ions in Mars-Sun-Electric field (MSE) coordinates, in which the  $X$ -axis points to the Sun, the  $Y$ -axis runs along the transverse compo-

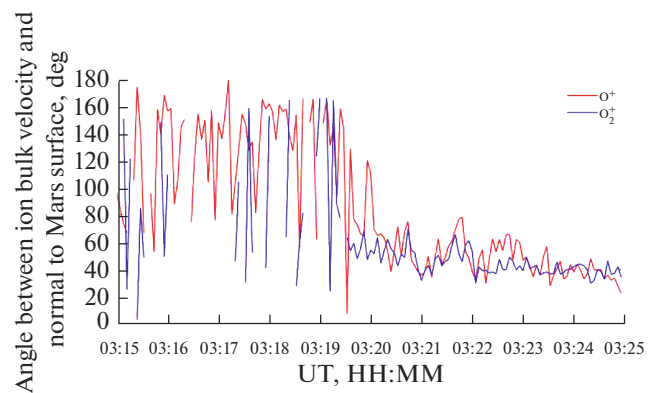


**Fig. 3.** The angle between ion bulk velocity and normal to the planet surface for  $O^+$  and  $O_2^+$  ions for the intersection shown in Fig. 2.

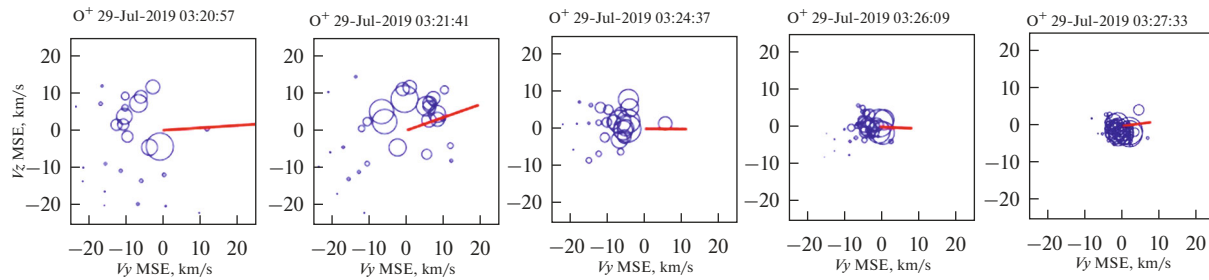


**Fig. 4.** Examples of oxygen ion distribution functions in velocity space ( $V_z$ – $V_y$ ). The size of the circle is proportional to the ion density in the phase space. The red lines show the projection of the magnetic field on the  $YZ$ -MSE plane.

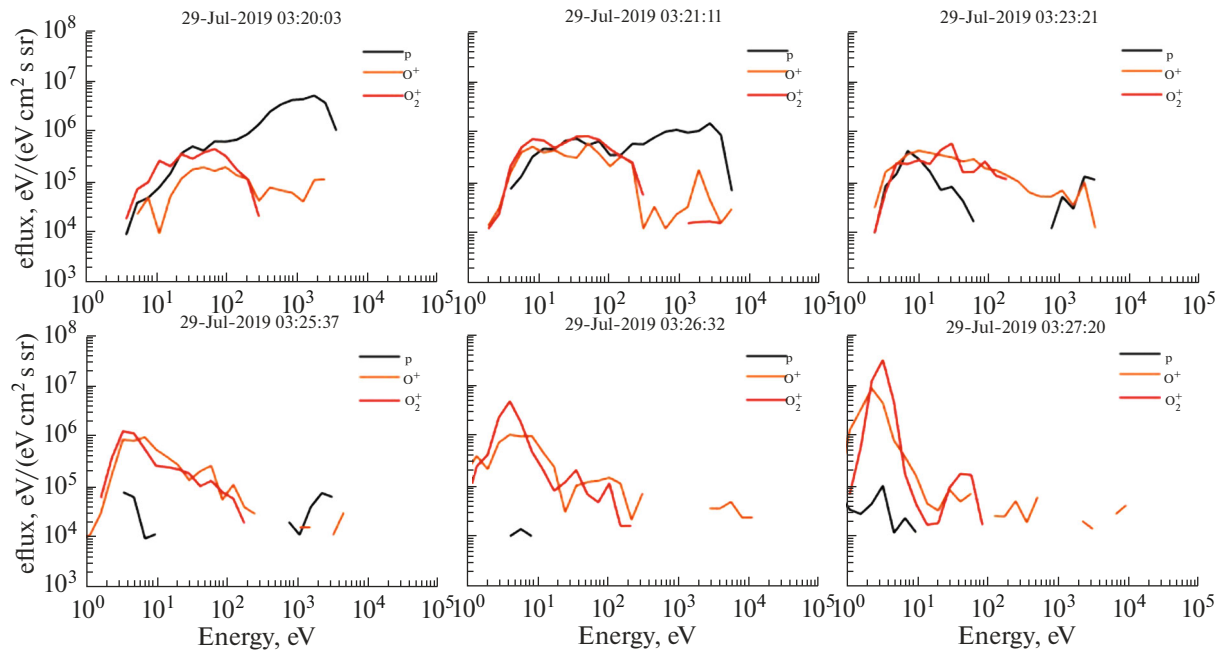


**Fig. 5.**  $H^+$ ,  $O^+$  and  $O_2^+$  energy spectra in the region adjacent to ionosphere.

ment of the interplanetary magnetic field in the solar wind, and the  $Z$ -axis runs along the motional electric field  $E = -(1/c)\mathbf{v} \times \mathbf{B}$ , approximately for the same time interval as in Fig. 2. The size of the circles shows the ion phase space density in the velocity space. It is observed that with increasing distance from the ionosphere, the  $Z$ -component of the velocities increases, indicating that the ions are accelerated by an external electric field.

The time interval  $\sim 03:25$ – $\sim 03:27$  approximately corresponds to the transition from the lower part of the ionosphere, where the  $n(O_2^+)/n(O^+)$  ratio is  $\sim 2$ , to the upper ionosphere with  $n(O_2^+)/n(O^+) \sim 1$  (see Fig. 2). At high altitudes, we observe an expansion of the ion distribution function in the direction of the motional electric field (03:24:27) and a further gradual acceleration of ions (03:21:41–03:20:57 UT).

Significant heating of oxygen ions in the outer part of the plasma envelope is clearly visible in Fig. 5, which shows the energy spectra of protons,  $O^+$  and  $O_2^+$  ions. It can be seen that, as spacecraft approaches the ionosphere, the ion spectra become less energetic. In the ionosphere ( $\sim 03:27:20$ ) the temperature of oxygen ions decreases.

Figure 6 shows another example of the daytime magnetosphere on July 31, 2019. The magnetosheath is shown on the left at a height of  $\sim 800$  km. The criteria for the location of the boundaries were presented in the discussion of the previous case in Fig. 1. In the case shown in Fig. 6, the magnetopause was crossed at 06:32:00 UT at a height of  $\sim 620$  km, as indicated by the ratio  $n_p/(n_p + n_h) \approx 0.5$ , a sharp drop in the ion energy (panel 1) and proton energy (panel 2), as well as an increase in the concentration and temperature of the flows of  $O^+$  and  $O_2^+$  ions (panels 3 and 4). The ion-

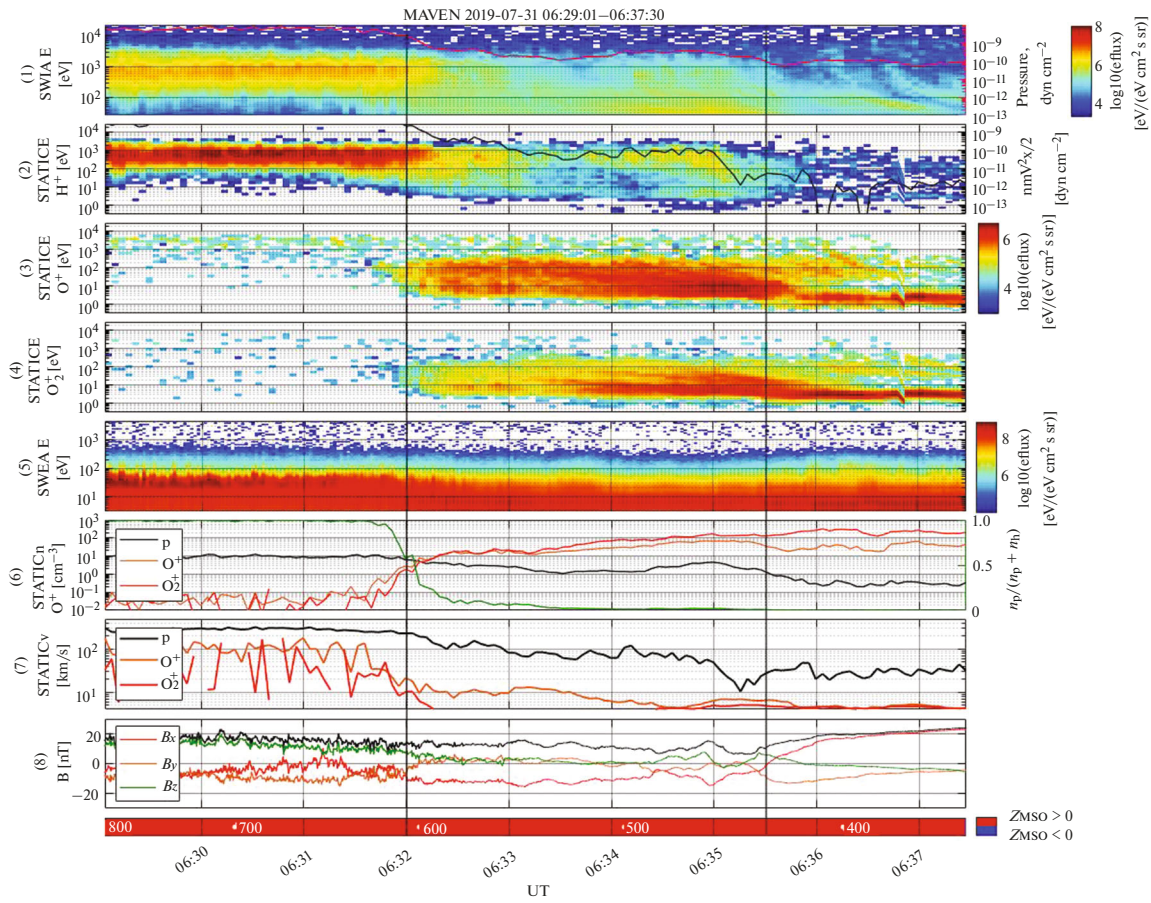


Fig. 6. See caption for Fig. 2.

opause is determined at an altitude of ~440 km at ~06:35:40 UT by the drop in the temperature of hot ions.

Just as was noted in the discussion of the previous example (Fig. 2), the change in the numerical ratio of  $O_2^+/O^+$  ions during the transition from the magnetosphere to the ionosphere occurs from 1–2 (panel 6) to 06:35:40 UT to ~5–10. Thus, in both cases, the change in the ratio  $n(O_2^+)/n(O^+)$  is about 5.

Figure 7 shows the directions of ion motion from the area in the magnetosheath to the ionosphere in projection to the normal to the magnetopause. It can be seen that the ions in the magnetosheath (up to ~06:31:45) predominantly move towards the planet, since the angle between the particle velocity and the outer normal to the planet is  $>90^\circ$ .

DAYSIDE MAGNETOSPHERE WITH PLUME

When a plume is present in the dayside magnetosheath, the plasma in the magnetosphere also contains populations of accelerated ionospheric ions and pick-up ions. The characteristics of ionospheric and

pick-up ions are very similar to those observed in the daytime magnetosphere in the absence of a plume. Figure 8 shows a typical example of such a structure of the magnetosphere.

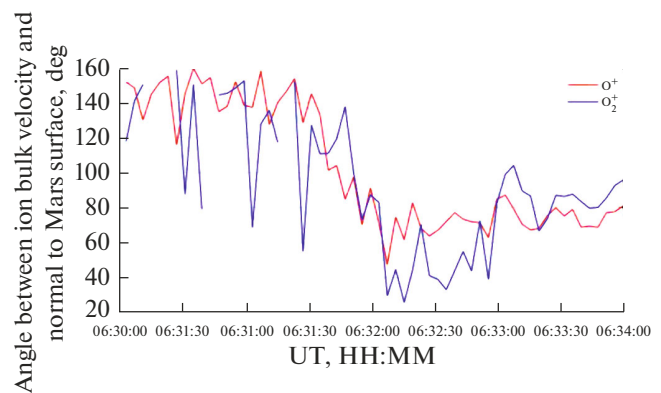


Fig. 7. The angle between bulk velocity and normal to the planet surface is less than  $90^\circ$ , showing the movement of plasma away from the planet.

**Table 1.** Ratio between number densities of  $O_2^+$  in  $O^+$  different regions

Parameter/region	$n(O_2^+)/n(O^+)$ in magnetopause	$n(O_2^+)/n(O^+)$ in magnetosphere	$n(O_2^+)/n(O^+)$ in ionosphere
Average value	1.8	2.4	5.8
Standard deviation	1.7	1.5	7.0

The plume is observed on 2019-08-03 UTC at 07:14:21–07:43:09 UTC (Fig. 8). It includes a significant part of the magnetosheath ( $\sim 07:14$  UT– $\sim 07:32:30$  UT) with a 10-times drop in ion dynamic pressure from  $1 \times 10^{-9}$  dyn/cm<sup>2</sup>, which we define as the boundary. A further sharp increase in the number of heavy ions and the ratio  $n_p/(n_p + n_h)$  (6th panel), an increase in the magnetic field  $B$ , and a decrease in magnetic field fluctuations (8th panel) confirm our identification of this boundary. The SZA at the magnetopause crossing was  $\sim 75^\circ$ .

Panels 3 and 4 show that the magnetosheath is filled with plume ions. This plasma structure, characterized by narrow energy spectra of heavy ions with a monotonic increase in energy, is formed by ions formed accelerated from extended exosphere and upper ionosphere under the influence of the electric field of the solar wind.

The angle between the bulk velocity of heavy ions and the normal to the surface of the planet, shown in Fig. 9 shows that these ions are moving away from the planet. This angle decreases as the ions accelerate in a motional electric field. A notable feature is that the

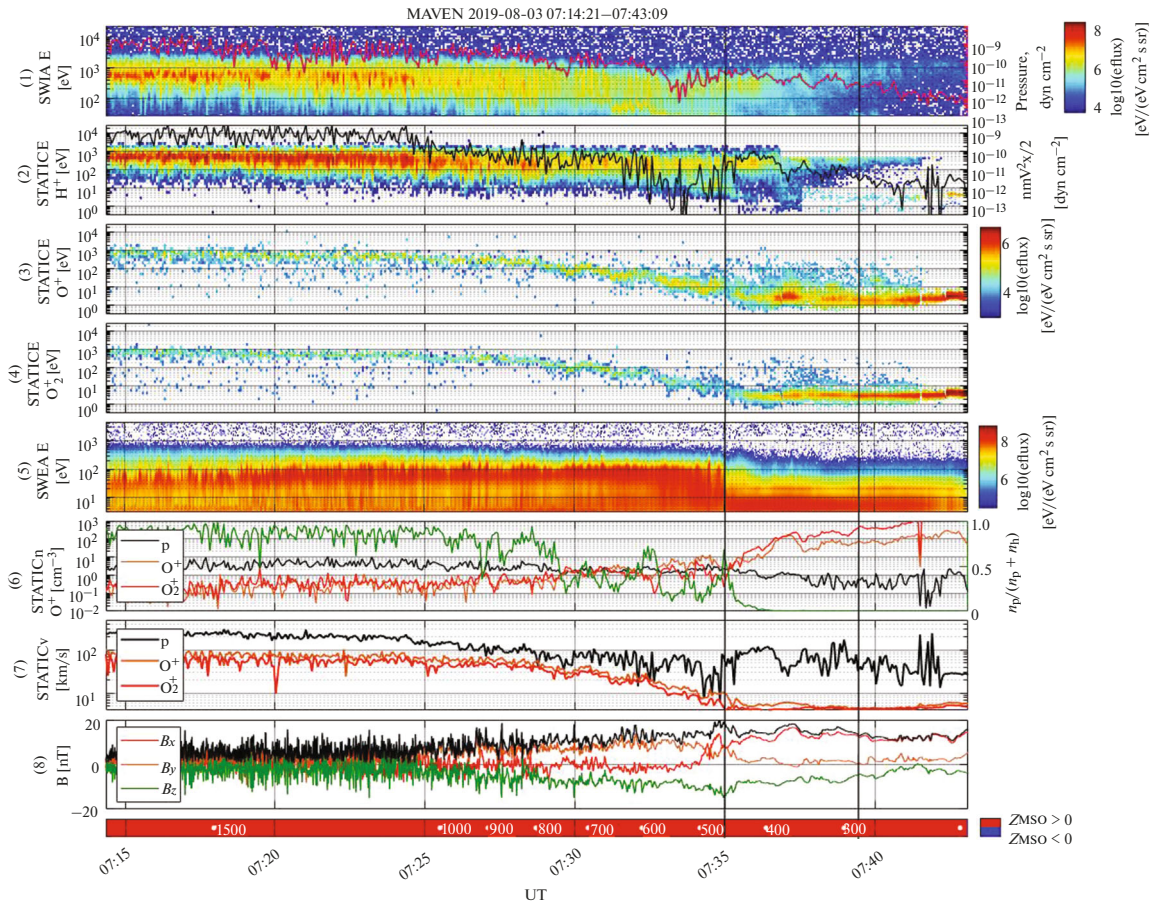


**Fig. 8.** Same as Fig. 2 shown for magnetosphere intersection on 3 August 2019. The ion plume is characterized by a narrow energy propagation of heavy ions with a monotonic increase in energy from the ionosphere through the magnetosheath.

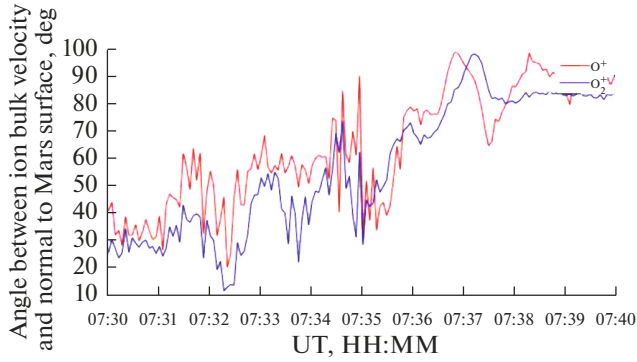


**Fig. 9.** The angle between ion bulk velocity and normal to the planet surface for  $O^+$  and  $O_2^+$  ions for the intersection shown in Fig. 8.

angle differs by  $\sim 10^\circ$  for both types of ions. This may be due to the different gyroradii of these ions.

Figure 10 shows the energy distributions of  $O^+$  and  $O_2^+$  ions during the detection of plume ions. These

energy distributions are very different from the distributions of picked-up ions (Fig. 5).

We also observe fluxes of the  $O^+$  and  $O_2^+$  pick-up ions with energies of  $10\text{--}10^3$  eV in the magnetosheath. Their densities in magnetosheath are rather small ( $\sim 0.1$  cm), however, they increase monotonically as the s/c move towards the ionosphere and reach  $\sim 20$  cm $^{-3}$  in its upper part.

Similarly, this ion component gradually decays during the transition from heated topside ionosphere to a regular ionosphere at  $\sim 07:42$  UT which indicate that the plume originate from the ionosphere.

Another example of the magnetosphere when plume is observed is shown in Fig. 11.

Using the ratio  $n_p/(n_p+n_h) \approx 0.5$  one puts the boundary at 12:05:00 UT. This time agrees with the drop of total magnetosheath ions dynamic pressure by factor of 10. This estimation indicate that the ions energies below of  $\sim 10^2$  energy fluxes of  $O^+$  and  $O_2^+$  ions are accelerated within magnetosphere.

The ratio of ion number densities  $O_2^+/O^+$  increases from a lower value of  $\sim 3$  in the magnetosphere to  $\sim 8$  in the ionosphere. It seems that it is determined by ionization by ultraviolet radiation and atmospheric pro-

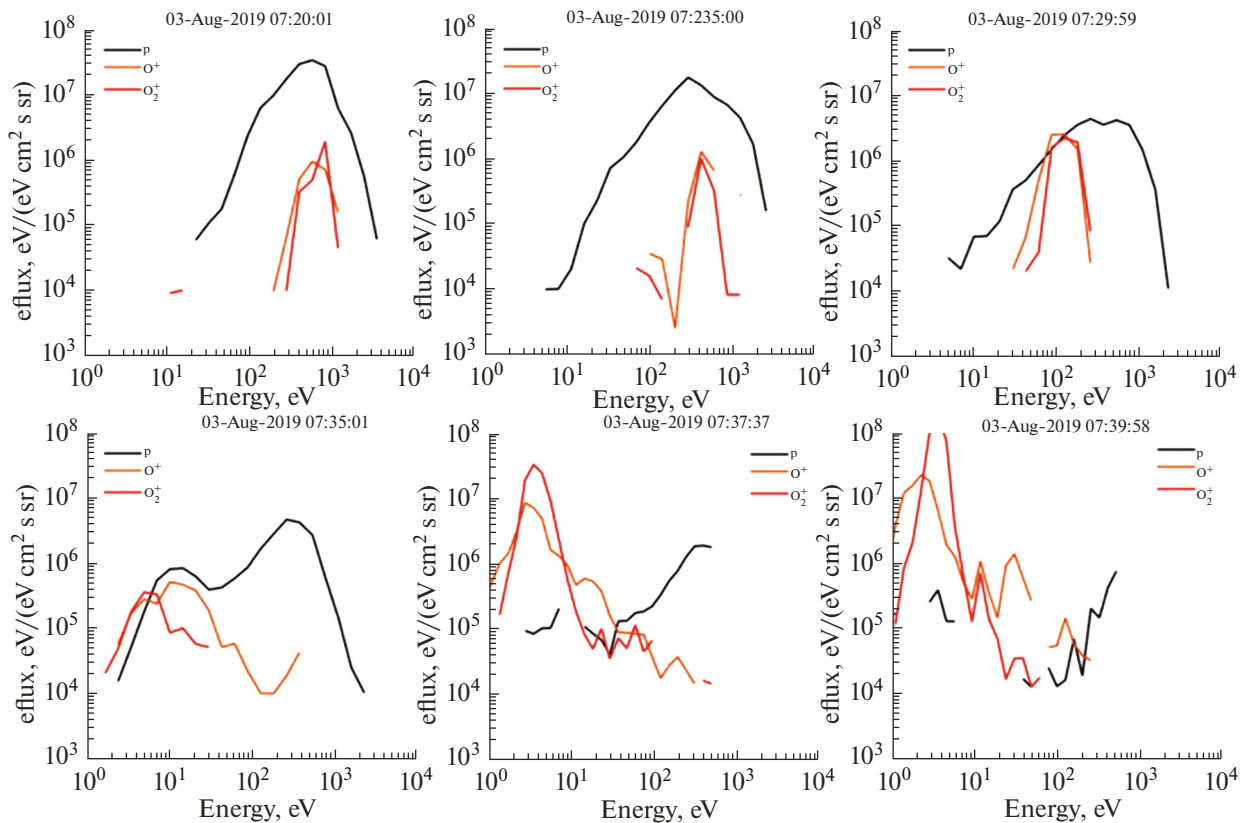


**Fig. 10.** Energy spectra of protons and heavy ions in different regions. Peaks in the low-energy part of the  $O^+$  and  $O_2^+$  spectra belong to the ion plume.



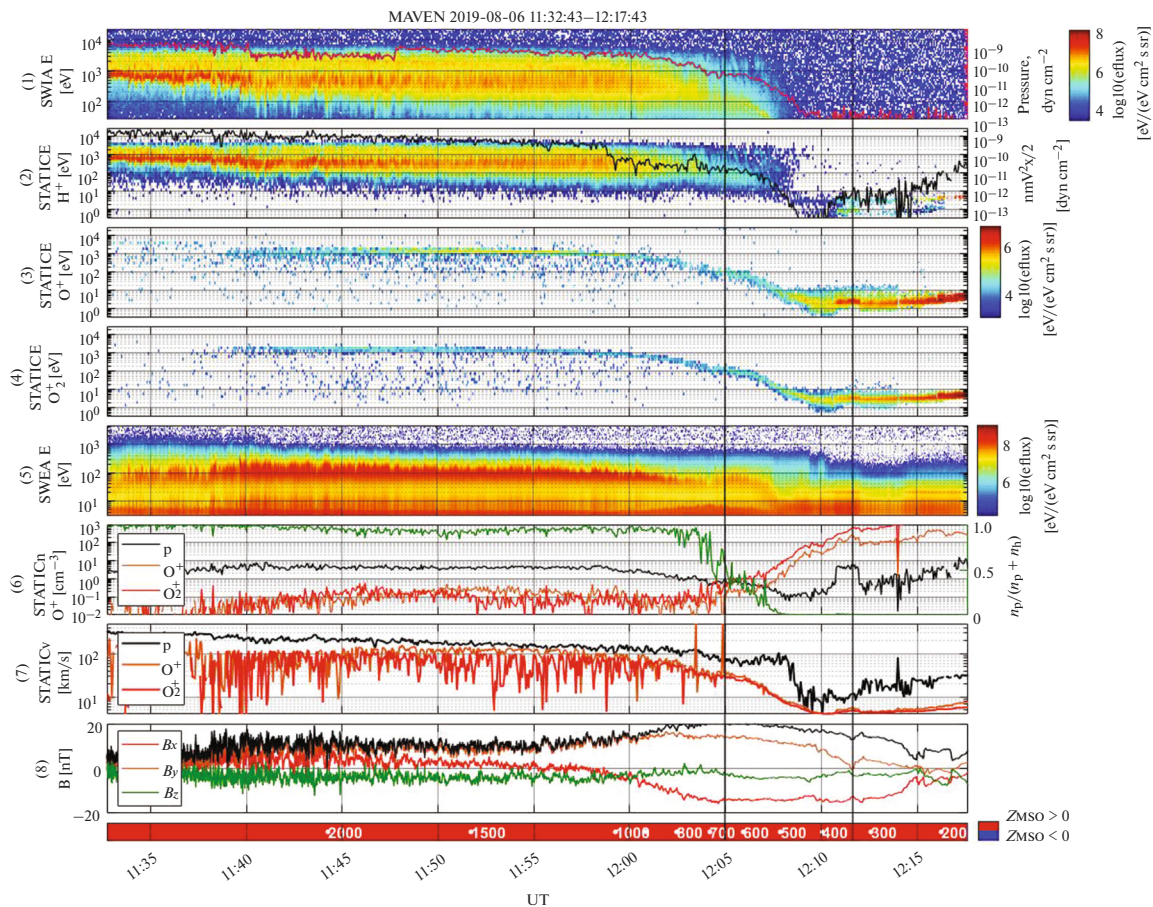


Fig. 11. Another example of a dayside magnetosphere with plume feature. See caption for Fig. 2.

cesses in the upper ionosphere, the same value of the ratio in the magnetosphere is determined mainly by ionization by ultraviolet radiation.

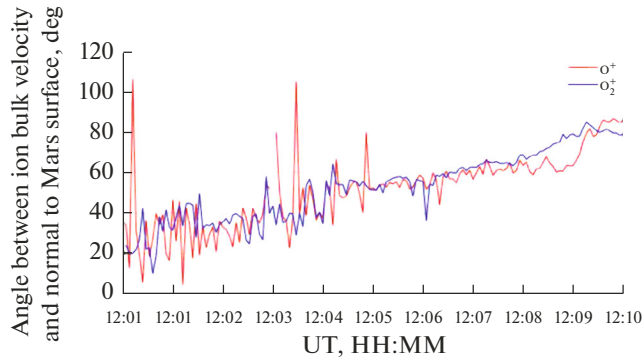
Like in the previous case of magnetosphere crossing with plume feature, bulk velocities of accelerated ions are directed away from the planet (see Fig. 12), and the angle between this direction and the planet surface normal decreases as particles accelerate.

Figure 13 and Table 1 show the average ratios of  $n(\text{O}_2^+)/n(\text{O}^+)$  over 3 observed sets of magnetospheres crossings considered in this paper. The scatter of numbers is significant the average values are distinct.

It is known that plume ions originate from ionosphere and are accelerated by motional electric field of the solar wind plasma (Dubinin et al., 2006 and references therein) making an important atmospheric loss channel (Dong et al., 2015). In order to make a rough estimation of the height from which the electric field starts to accelerate plume ions to the observed energy values we compared the measured energies in the plume with electric field potential drop between the spacecraft position and height of 420 km above the surface of Mars in the  $+Z_{\text{MSE}}$  direction (Fig. 14) for the crossing presented in Fig. 8. This height of 420 km was

selected for best fitting between the two curves in Fig. 8 and is also close to the upper boundary of the ionosphere. The blue line shows the energy value with the highest measured differential energy flux at a certain moment of time. The motional electric field was calculated from the measurements upstream from the Martian bow shock as  $E = -(1/c)[V_{\text{SW}} \times B]$ , where  $V_{\text{SW}}$  is the measured by the STATIC proton bulk velocity averaged over the time interval from 7:00 to 7:10 UT, and  $B$  is magnetic field vector measured by MAG and averaged over the same time interval.

In general, the curves are in a good agreement with each other. Discrepancy between the curves seen in energies higher than 100 eV are probably caused by cycloidal motion of the plume ions, as a result of that the ions are detected further from spacecraft than predicted by our simple model and, accordingly, cover a longer path gaining an additional energy. It is seen that ions in the model are significantly under-accelerated in the left part of the figure, compared with the measured ion energy. It may be apparently related with the electric field in the magnetosheath that has not been taken into account and that is stronger than the upstream electric field. The proposed model can also



**Fig. 12.** The angle between ion bulk velocity and normal to the planet surface for  $O^+$  and  $O_2^+$  ions for the intersection shown in Fig. 11.

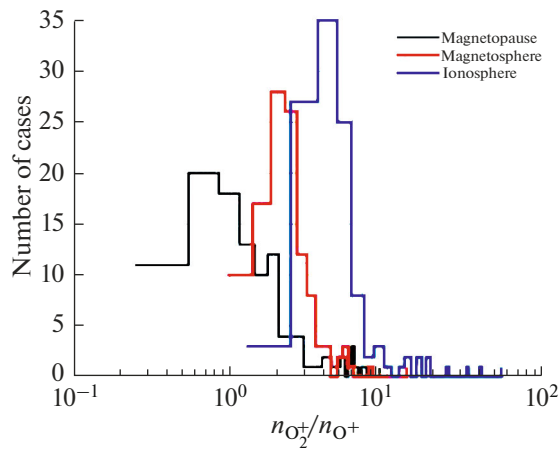


**Fig. 13.** Distributions of  $n(O_2^+)/n(O^+)$  in the analyzed orbits in magnetopause, magnetosphere and upper ionosphere.

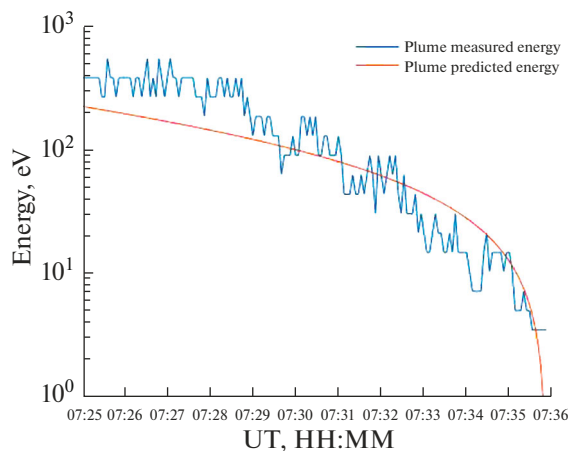


**Fig. 14.** Comparison of energy in the plume (blue) and predicted energy assuming that plume ions are accelerated by the induced electric field of the solar wind from a height of 420 km with zero initial energy (red).

be used for estimation of the height from which the electric field starts to accelerate ionospheric ions.

## CONCLUSIONS

This analysis of plasma and magnetic field are bases on the MAVEN data. The measurements of plasma and magnetic field at 115 passes at altitude above  $\sim 300$  km in the north hemisphere at solar-zenith angles  $\sim 70^\circ$  within time interval July 27, 2019–October 31, 2019 were analyzed. Previous analysis of other dayside sets of regions between the dayside magnetosheath and ionosphere did not include the cases with the plume. In current selection of passes of dayside magnetosphere we included the plume cases and it was found that the ratio of cases without the plume (cases A) to the cases with plume (cases B) was approximately 50%.

Previous analysis (Vaisberg and Shuvalov, 2021) did not reveal any cases of direct interaction of magnetosheath on the dayside of the planet with the ionosphere. The layer between magnetosheath and ionosphere was filled with a mixture of heated ionospheric  $O^+$  and  $O_2^+$  ions and picked-up and accelerated exospheric ions by the solar wind. This layer was called the Martian dayside magnetosphere.

A more detailed analysis of the magnetospheric plasma showed fairly regular profiles “A” of  $O^+$  and  $O_2^+$  ions number densities and their ratios (see. Figs. 2 and 6): (1) initial sharp increase in the magnetopause from  $O_2^+/O^+ \sim 1$ , (2) smooth or two-step increase by 1.5–3 times with change of  $O_2^+/O^+ \sim (1-2)$  and (3) short rise of  $O^+$ , especially  $O_2^+$ , significant rise of  $O_2^+/O^+$  ratio, (4) slow rise of  $O_2^+$  and  $O^+$  ions number density with values typical for the upper ionosphere.

In “B” cases (plume, Figs. 8 and 11) one can see a heated layer of the ionosphere above the cold ionosphere: average increase in ion energy up to  $\sim 10$  eV in Fig. 8 and up to  $\sim 10^2$  eV in Fig. 11. These boundaries correspond to the location of obstacles, which correspond to the dips in the energy flux of the magnetosphere for both cases. Figures 9 and 12 confirm the location of the boundaries between magnetospheric flows and obstacles.

In short, plume originating on the dayside of Mars is involved in the formation of a region that plays the same role as the dayside magnetosphere, being an obstacle between the magnetosphere and the ionosphere.

## ACKNOWLEDGMENTS

O. Vaisberg would like to thank the MAVEN team and especially MAVEN project leader Professor Bruce Jakoski for the pleasure of working with MAVEN data.

## FUNDING

This work was supported by the Russian Science Foundation (grant no. 21-42-04404). MAVEN data is publicly available at <https://pds.nasa.gov>.

## CONFLICT OF INTEREST

The authors declare that they have no conflicts of interest.

## REFERENCES

- Bogdanov, A.V. and Vaisberg, O.L., Structure and variations of solar wind–Mars interaction region, *J. Geophys. Res.*, 1975, vol. 80, no. 4, pp. 487–494. <https://doi.org/10.1029/JA080i004p00487>
- Böswetter, A., Simon, S., Bagdonat, T., Motschmann, U., Fränz, M., Roussos, E., Krupp, N., Woch, J., Schüle, J., Barabash, S., and Lundin, R., Comparison of plasma data from ASPERA-3/Mars-Express with a 3-D hybrid simulation, *Ann. Geophys.*, 2007, vol. 25, pp. 1851–1864.
- Connerney, J.E.P., Espley, J.R., Lawton, P., Murphy, S., Odom, J., Oliverson, R., and Sheppard, D., The MAVEN magnetic field investigation, *Space Sci. Rev.*, 2015, vol. 195, pp. 257–291. <https://doi.org/10.1007/s11214-015-0169-4>
- Dessler, A.J., *Ionizing plasma flux in the Martian upper atmosphere, Atmospheres of Venus and Mars*, New York: Gordon and Breach, 1968.
- Dolginov, Sh.Sh., *The magnetosphere of Mars, Physics of the Solar Planetary Environment 2*, Williams, D.J., Ed., Boulder, CA: Am. Geophys. Union, 1976, p. 872.
- Dong, Y., Fang, X., Brain, D.A., McFadden, J.P., Halekas, J.S., Connerney, J.E., Curry, S.M., Harada, Y., Luhmann, J.G., and Jakosky, B.M., Strong plume fluxes at Mars observed by MAVEN: An important planetary ion escape channel, *Geophys. Res. Lett.*, 2015, vol. 42, no. 21, pp. 8942–8950. <https://doi.org/10.1002/2015GL065346>
- Dryer, M. and Heckman, G.R., Application of the hypersonic analog to the standing shock of Mars, *Sol. Phys.*, 1967, no. 2, pp. 112–124.
- Dubinin, E., Lundin, R., Franz, M., Woch, J., Barabash, S., Fedorov, A., Winningham, D., Krupp, N., Sauvaud, J.-A., Holmström, M., Andersson, H., Yamachi, M., Grigoriev, A., Thocaven, J.-J., Frahm, R., et al., Electric fields within the Martian magnetosphere and ion extraction: ASPERA-3 observations, *Icarus*, 2006, vol. 182, no. 2, pp. 337–342.
- Dubinin, E., Modolo, R., Fraenz, M., Woch, J., Chanteur, G., Duru, F., Akalin, F., Gurnett, D., Lundin, R., Barabash, S., Winningham, J.D., Frahm, R., Plaut, J.J., and Picardi, G., Plasma environment of Mars as observed by simultaneous MEX-ASPERA-3 and MEX-MARSIS observations, *J. Geophys. Res.*, 2008a, vol. 113, no. A10, id. A10217. <https://doi.org/10.1029/2008JA013355>
- Dubinin, E., Modolo, R., Fraenz, M., Woch, J., Duru, F., Akalin, F., Gurnett, D., Lundin, R., Barabash, S., Plaut, J.J., and Picardi, G., Structure and dynamics of the solar wind/ionosphere interface on Mars: MEX-ASPERA-3 and MEX-MARSIS observations, *Geophys. Res. Lett.*, 2008b, vol. 35, no. 11, id. L11103. <https://doi.org/10.1029/2008GL033730>
- Dubinin, E., Fränz, M., Fedorov, A., Lundin, R., Edberg, N., Duru, F., and Vaisberg, O., Ion energization and escape on Mars and Venus, *Space Sci. Rev.*, 2011, vol. 162, pp. 173–211. <https://doi.org/10.1007/s11214-011-9831-7>
- Espley, J.R., The Martian magnetosphere: Areas of unsettled terminology, *J. Geophys. Res.: Space Phys.*, 2018, vol. 123, pp. 4521–4525. <https://doi.org/10.1029/2018JA025278>
- Gringauz, K.I., Bezrukikh, V.V., Verigin, M.I., and Remizov, A.P., On electron and ion components of plasma in the antisolar part of near-Mars space, *J. Geophys. Res.*, 1976, vol. 81, pp. 3349–3352.
- Halekas, J.S., Taylor, E.R., Dalton, G., Johnson, G., Curtis, D.W., McFadden, J.P., Mitchell, D.L., Lin, R.P., and Jakosky, B.M., The solar wind ion analyzer for MAVEN, *Space Sci. Rev.*, 2015, vol. 195, pp. 125–151. <https://doi.org/10.1007/s11214-013-0029-z>
- Halekas, J.S., Ruhunusiri, S., Harada, Y., Collinson, G., Mitchell, D.L., Mazelle, C., McFadden, J.P., Connerney, J.E.P., Espley, J.R., Eparvier, F., Luhmann, J.G., and Jakosky, B.M., Structure, dynamics, and seasonal variability of the Mars–solar wind interaction: MAVEN solar wind ion analyzer in-flight performance and science results, *J. Geophys. Res.: Space Phys.*, 2017, vol. 122, no. 1, pp. 547–578. <https://doi.org/10.1002/2016JA023167>
- Halekas, J.S., McFadden, J.P., Brain, D.A., Luhmann, J.G., DiBarccio, G.A., Connerney, J.E.P., Mitchell, D.L., and Jakosky, B.M., Structure and variability of the Martian ion composition boundary layer, *J. Geophys. Res.*, 2018, vol. 123, no. 10, pp. 8439–8458. <https://doi.org/10.1029/2018JA025866>
- Holmberg, M.K.G., Andre, N., Garner, P., Modolo, R., Andersson, L., Halekas, J., Mazelle, C., Steckiewicz, M., Genot, V., Fedorov, A., Barabash, S., and Mitchell, D.L., Maven and MEX multi-instrument study of the dayside of the Martian induced magnetospheric structure revealed by pressure analyses, *J. Geophys. Res.*, 2019, vol. 124, no. 11, pp. 8564–8589. <https://doi.org/10.1029/2019JA026954>
- Jakosky, B.M., Grebowsky, J.M., Luhmann, J.L., and Brain, D.A., Initial results from the MAVEN mission to Mars, *Geophys. Res. Lett.*, 2015, vol. 42, no. 21, pp. 8791–8802. <https://doi.org/10.1002/2015GL065271>
- Kallio, E. and Koskinen, H., A test particle simulation of the motion of oxygen ions and the solar wind protons, *J. Geophys. Res.*, 1999, vol. 104, no. A1, pp. 557–559. <https://doi.org/10.1029/1998JA900043>
- Kallio, E., Fedorov, A., Budnik, E., Säles, T., Janhunen, P., Schmidt, W., Koskinen, H., Riihelä, P., Barabash, S., Lundin, R., Holmstrom, M., Gunell, H., Brinkfeldt, K., Futaana, Y., Andersson, H., et al., Ion escape from Mars: Comparison of a 3-D hybrid simulation with Mars Express IMA/ASPERA-3 measurements, *Icarus*, 2006, vol. 182, no. 2, pp. 350–359. <https://doi.org/10.1016/j.icarus.2005.09.018>
- Kallio, E., Fedorov, A., Budnik, E., Barabash, S., Jarvinen, R., and Janhunen, P., On the properties of O<sup>+</sup> and O<sub>2</sub><sup>+</sup> ions in a hybrid model and in Mars Express IMA/ASPERA-3

- data: A case study, *Planet. Space Sci.*, 2008, vol. 56, no. 9, pp. 1204–1213.  
<https://doi.org/10.1016/j.pss.2008.03.007>
- Liemohn, M.W., Johnson, B.C., Fraenz, M., and Barabash, S., Mars Express observations of high altitude planetary ion beams and their relation to the “energetic plume” loss channel, *J. Geophys. Res.: Space Phys.*, 2014, vol. 119, no. 12, pp. 9702–9713.  
<https://doi.org/10.1002/2014JA019994>
- McFadden, J.P., Kortmann, O., Curtis, D., Dalton, G., Johnson, G., Abiad, R., Sterling, R., Hatch, K., Berg, P., Tiu, C., Gordon, D., Heavner, S., Robinson, M., Marckwordt, M., Lin, R., et al., MAVEN Supra-Thermal and Thermal Ion Composition (STATIC) instrument, *Space Sci. Rev.*, 2015, vol. 195, pp. 199–256.  
<https://doi.org/10.1007/s11214-015-0175-6>
- Mitchell, D.L., Mazelle, C., Sauvaud, J.-A., Thocaven, J.-J., Rouzaud, J., Federov, A., Rouger, P., Toubanc, D., Taylor, E., Gordon, D., Robinson, M., Heavner, S., Turin, P., Diaz-Aguado, M., Curtis, D.W., et al., The MAVEN Solar Wind Electron Analyzer (SWEA), *Space Sci. Rev.*, 2016, vol. 200, no. 1, pp. 495–528.  
<https://doi.org/10.1007/s11214-015-0232-1>
- Szego, K., Klimov, S., Kotova, G.A., Livi, S., Rosenbauer, H., Skalsky, A., and Verigin, M.I., On the dayside region between the shocked solar wind and the ionosphere of Mars, *J. Geophys. Res.*, 1998, vol. 103, no. A5, pp. 9101–9111.  
<https://doi.org/10.1029/98JA00103>
- Vaisberg, O. and Shuvalov, S., Properties and sources of the dayside Martian magnetosphere, *Icarus*, 2021, vol. 354, id. 114085.  
<https://doi.org/10.1016/j.icarus.2020.114085>
- Vaisberg, O.L., Bogdanov, A.V., Smirnov, V.N., and Romanov, S.A., *On the nature of solar-wind–Mars interaction, Solar Wind Interaction with Planets Mercury, Venus and Mars*, Ness, N.F., Ed., Washington, DC: Natl. Aeronaut. Space Admin., 1976, p. 21.
- Vaisberg, O.L., Ermakov, V.N., Shuvalov, S.D., Zelenyi, L.M., Znobishchev, A.S., and Dubinin, E.M., Analysis of dayside magnetosphere of Mars: High mass loading case as observed on MAVEN spacecraft, *Planet. Space Sci.*, 2017, no. 147, pp. 28–37.
- Van Allen, J.A., Frank, L.A., Krimigis, S.M., and Hills, H.K., Absence of Martian radiation belts and implications thereof, *Science*, 1965, vol. 149, no. 3689, pp. 1228–1233.